

## Supporting Information

### Transforming Petroleum asphalt into Carbon Fibers and Related Metal/Oxide Composites by Electrospinning Synthesis

*Ying Gao<sup>a</sup>, Yang Li<sup>c</sup>, Qiang Niu<sup>b</sup>, Pengfei Zhang<sup>a,c\*</sup>*

*<sup>a</sup> School of Chemistry and Chemical Engineering, Shanghai Jiao Tong University, Shanghai  
200240, China*

*<sup>b</sup> National Enterprise Technology Center, Inner Mongolia Erdos Electric Power and  
Metallurgy Group Co., Ltd., Ordos 016064, Inner Mongolia, China*

*<sup>c</sup> State Key Laboratory of High-efficiency Utilization of Coal and Green Chemical Engineering,  
College of Chemistry and Chemical Engineering, Ningxia University, Yinchuan 750021, China*

*E-mail: pfzhang@nxu.edu.cn*

*\* Corresponding authors: chemistryzpf@sjtu.edu.cn*

## 1. Experimental section

### 1.1 Chemicals

Materials and Reagents: All chemical compounds, including Polyacrylonitrile (PAN), N,N-Dimethylacetamide (DMA), Cobalt tetramethoxyphenylporphyrin ( $C_{48}H_{36}CoN_4O_4$ ), Nickel(II) meso-tetraphenylporphine ( $C_{44}H_{28}N_4Ni$ ), Manganese(III) meso-tetraphenylporphine chloride ( $C_{44}H_{28}ClMnN_4$ ), Copper(II) tetramethoxyphenylporphyrin ( $C_{48}H_{36}CuN_4O_4$ ), Hematin chloride ( $C_{34}H_{32}C_1N_4FeO_4$ ), Nickel(II) Nitrate Hexahydrate ( $Ni(NO_3)_2 \cdot 6H_2O$ ), Cobalt(II) Nitrate Hexahydrate ( $Co(NO_3)_2 \cdot 6H_2O$ ), Ferric Nitrate Nonahydrate ( $Fe(NO_3)_3 \cdot 9H_2O$ ), Manganese(II) Nitrate Tetrahydrate ( $Mn(NO_3)_2 \cdot 4H_2O$ ), MnO (~100nm), Al<sub>2</sub>O<sub>3</sub> (~20nm) and CaO (~200nm), were obtained from Energy Chemical. Asphalt (10# asphalt), were obtained from Riton Technology Co., Ltd. in Nanjing. All chemicals were purchased from commercial source and used as received without further purification.

### 1.2 Preparation

#### 1.2.1 preparation of Asphalt-based carbon fibers

Typically, 4.0 g of asphalt was dissolved to 30 mL DMA under magnetic stirring. 2.0 g of PAN was added to the above solution. After stirred overnight at 60 °C, the resulted polymer solution was electrospun under the conditions of 30 °C, the humidity <25%, applied voltage of 22 kV, a spinning speed of 0.7 mL h<sup>-1</sup>, and the distance of 15 cm between the receiving aluminum foil and the needle. The electrospun nanofiber films were collected on the aluminum foil and stabilized in a muffle furnace at 220 °C for 3 h, and then annealed at 800 °C for 1 h under the N<sub>2</sub> atmosphere. The High-Asphalt-Content Carbon Fibers (ACFs) was obtained finally, and denoted as APA-2.

Using identical procedures, the APA-1.75 and APA-3 were synthesized. APA-1.75 and APA-3 means the mass ratio of asphalt and PAN was 1.75 and 3, respectively.

### *1.2.2 preparation of the Metalloporphyrin@APA-2*

Typically, 4.0 g of asphalt and 25mg  $C_{48}H_{36}CoN_4O_4$  was dissolved to 30 mL DMA under magnetic stirring. 2.0 g of PAN was added to the above solution. After stirred overnight at 60 °C, the resulted polymer solution was electrospun under the conditions of 30 °C, the humidity <25%, applied voltage of 22 kV, a spinning speed of 0.7 mL h<sup>-1</sup>, and the distance of 15 cm between the receiving aluminum foil and the needle. The electrospun nanofiber films were collected on the aluminum foil and stabilized in a muffle furnace at 220 °C for 3 h, and then annealed at 800 °C for 1 h under the N<sub>2</sub> atmosphere. The Metalloporphyrin@APA-2 was obtained finally, and denoted as Co\*.

Using identical procedures, the Ni\*, Fe\* and Mn\* were synthesized.

### *1.2.3 preparation of the Nitrate@APA-2*

Typically, 4.0 g of asphalt and 25mg  $Mn(NO_3)_2 \cdot 4H_2O$  was dissolved to 30 mL DMA under magnetic stirring. 2.0 g of PAN was added to the above solution. After stirred overnight at 60 °C, the resulted polymer solution was electrospun under the conditions of 30 °C, the humidity <25%, applied voltage of 22 kV, a spinning speed of 0.7 mL h<sup>-1</sup>, and the distance of 15 cm between the receiving aluminum foil and the needle. The electrospun nanofiber films were collected on the aluminum foil and stabilized in a muffle furnace at 220 °C for 3 h, and then annealed at 800 °C for 1 h under the N<sub>2</sub> atmosphere. The Nitrate@APA-2 was obtained finally, and denoted as Mn.

Using identical procedures, the Ni, Fe and Co were synthesized.

#### *1.2.4 preparation of the Oxides@APA-2*

Typically, 4.0 g of asphalt and 25mg MnO was dissolved to 30 mL DMA under magnetic stirring. 2.0 g of PAN was added to the above solution. After stirred overnight at 60 °C, the resulted polymer solution was electrospun under the conditions of 30 °C, the humidity <25%, applied voltage of 22 kV, a spinning speed of 0.7 mL h<sup>-1</sup>, and the distance of 15 cm between the receiving aluminum foil and the needle. The electrospun nanofiber films were collected on the aluminum foil and stabilized in a muffle furnace at 220 °C for 3 h, and then annealed at 900 °C for 1 h under the N<sub>2</sub> atmosphere. The Oxides@APA-2 was obtained finally, and denoted as MnO.

Following the same procedure, CaO- and Al<sub>2</sub>O<sub>3</sub>-doped samples were prepared using CaO and Al<sub>2</sub>O<sub>3</sub> instead of MnO, with a carbonization temperature of 800 °C for 1 h. For the preparation of oxide-doped spinning solutions, 25 mg of MnO (~100 nm), CaO (~200 nm), or Al<sub>2</sub>O<sub>3</sub> (~20 nm) was added to 30 mL of DMA and stirred magnetically to form a homogeneous suspension. These oxides were used in the solid state and not fully dissolved in DMA.

#### *1.2.5 preparation of contrast samples*

Typically, 4.0 g of asphalt or PAN was individually annealed at 800 °C for 1 h under the N<sub>2</sub> atmosphere, and the resulting products were denoted as AP and PAN, respectively. It is worth noting that the carbonized PAN formed a dense, hard monolithic block, which could not be dispersed into a uniform ink suitable for electrocatalytic testing. Moreover, 4.0 g of asphalt and 2.0 g of PAN were first ball-milled together for 30 minutes and then carbonized at 800 °C under N<sub>2</sub> flow in a tube furnace. The resulting sample was denoted as BM30.

### *1.3 Material characterization*

X-ray diffraction (XRD) analysis utilized the Rigaku Ultima IV equipment. The specific surface areas (SSA) and porosity were evaluated through nitrogen adsorption-desorption measurements performed with a Micromeritics TriStar II 3020 apparatus. The elemental compositions of the catalyst were precisely determined using inductively coupled plasma optical emission spectroscopy (ICP-OES) with a Thermo Fisher iCAP PRO (OES) instrument. The ZEISS GeminiSEM 300 scanning electron microscope (SEM) was used for sample morphology and energy spectrum mapping. High-resolution Transmission electron microscopy (HRTEM) images were obtained using a JEOL JEM 2100 device and a ZEISS GeminiSEM 300 instrument. High-angle annular dark field imaging-scanning transmission electron microscopy (HAADF-STEM) and energy-dispersive. Fourier transform infrared (FT-IR) spectra were performed by using Nicolet iS50 spectrometer with a KBr pellet in the range from 400 to 4000  $\text{cm}^{-1}$ . Thermogravimetric analysis (TGA, DTG-60H) was conducted in air with a heating rate of 5  $^{\circ}\text{C min}^{-1}$  in the temperature range from 25 to 850  $^{\circ}\text{C}$ . Specific elemental compositions, bonding types, and other chemical structures of the samples were analyzed by X-ray photoelectron spectroscopy (XPS, Thermo ESCALAB 250XI X) using an Al-K $\alpha$  monochromatic source with energy of 1486.6 eV. Raman spectroscopy (Laman, Lab RAM HR, 532 nm laser) was used to analyze the changes of binding bonds in the samples.

### *1.4 Electrochemical Measurements*

All the electrochemical measurements were performed in a standard three-electrode cell at room temperature using an electrochemical workstation (CHI660E), in which the

sample to be tested was used as the working electrode (geometric area: 1 cm<sup>2</sup>), a carbon rod as the counter electrode, and a Hg/HgO electrode (MOE, filled with 1 mol/L KOH solution) as the reference electrode. Electrodes for OER were prepared by uniformly casting 100 μL of catalysts-H<sub>2</sub>O/ethanol-Nafion suspension (5 mg catalyst, 350 μL of deionized water, 700 μL of ethanol, 80 μL of 5% Nafion, ) on carbon cloth (1 cm<sup>2</sup>) after ultrasound for 15 min. All linear sweep voltammetry (LSV) curves for the OER were obtained at a scan rate of 5 mV/s. The potentials were converted to the potentials referring to the RHE, according to  $E(\text{RHE}) = E(\text{MOE}) + 0.059 \text{ pH} + 0.098 \text{ V}$ . Tafel plots were recorded with the linear portions at low overpotential fitted to the Tafel equation. Tafel slopes are calculated based on the equation:

$$\eta = b \log j$$

Where  $\eta$  is the overpotential,  $b$  is the Tafel slope and  $j$  is the current density.

The intercept on the real axis and the semicircle in the Nyquist plot are considered as the resistance of electrolyte ( $R_s$ ), the charge transfer resistance ( $R_1$ ) and the catalysts and solution resistance ( $R_2$ ), respectively. All resistances were fitted by *Zview* software. The equivalent circuit consists of a capacitor and a resistor in parallel. Electrochemical impedance spectroscopy (EIS) measurements were conducted at an overpotential of 500 mV with a potential perturbation amplitude of 5 mV in the range of 10 kHz to 0.1 Hz. The electrolyte resistance was measured using EIS and used for *iR* compensation using the equation,  $E_{iR\text{-corrected}} = E_{\text{original}} - (I \times R_s)$ . The electrochemical double-layer capacitance ( $C_{dl}$ ) was estimated by cyclic voltammetry (CV) in the potential range of 0.989–1.139 V versus RHE without faradaic current at scan rates of 10, 20, 40, 50, 100 mV s<sup>-1</sup>, respectively. The current density differences [ $\Delta j = (j_a - j_c)$ ] were plotted against scan rates, a linear trend was constructed.

**Tables :****Table S1** The results of elemental analysis

Samples	C	H	O	N	S
Mn*	81.85	1.17	4.61	8.12	0.51
Mn	81.85	1.34	5.05	7.17	0.83

**Table S2** TEM-EDS area analysis of APA-2 sample (corresponding to Fig. 1(h))

Element	Line	Atomic Fraction (%)	Mass Fraction (%)
C	K	94.44	93.20
N	K	3.11	3.58
O	K	2.45	3.22
Total		100	100

**Table S3** SEM-EDS area analysis of Mn\* sample (corresponding to Fig. S25)

Element	Line	Wt%	Wt% Sigma	At%
C	K $\alpha$	87.52	0.76	89.64
N	K $\alpha$	8.34	0.66	7.32
O	K $\alpha$	3.87	0.13	2.98
Mn	L $\alpha$	0.27	0.46	0.06
Total		100		100

**Table S4** SEM-EDS area analysis of Ni sample (corresponding to Fig. S26)

Element	Line	Wt%	Wt% Sigma	At%
C	K $\alpha$	88.50	0.66	90.58
N	K $\alpha$	7.95	0.67	6.97
O	K $\alpha$	3.05	0.11	2.34
Ni	L $\alpha$	0.51	0.10	0.11
Total		100		100

**Table S5** TEM-EDS area analysis of Mn sample (corresponding to Fig. S27)

Element	Line	Atomic Fraction (%)	Mass Fraction (%)
C	K	83.86	79.85
N	K	4.09	4.54
O	K	11.95	15.16
Mn	K	0.10	0.45
Total		100	100

**Table S6** SEM-EDS area analysis of MnO sample (corresponding to Fig. S30)

Element	Line	Wt%	Wt% Sigma	At%
C	K $\alpha$	91.50	0.95	93.71
N	K $\alpha$	2.19	0.83	1.92
O	K $\alpha$	5.43	0.18	4.18
Mn	L $\alpha$	0.87	0.57	0.20
Total		100		100

**Table S7** SEM-EDS area analysis of MnO sample (corresponding to Fig. S31)

Element	Line	Wt%	Wt% Sigma	At%
C	K $\alpha$	91.45	0.98	93.12
N	K $\alpha$	2.41	0.86	2.62
O	K $\alpha$	5.34	0.21	4.08
Mn	L $\alpha$	0.80	0.51	0.18
Total		100		100

**Table S8** SEM-EDS area analysis of CaO sample (corresponding to Fig. S34)

Element	Line	Wt%	Wt% Sigma	At%
C	K $\alpha$	86.35	0.66	88.78
N	K $\alpha$	7.31	0.69	6.45
O	K $\alpha$	6.07	0.13	4.69
Ca	K $\alpha$	0.27	0.04	0.08
Total		100		100

**TableS9** The structure properties of all samples<sup>a</sup>

Samples	$S_{\text{BET}}$ (m <sup>2</sup> /g)	Pore volume <sup>b</sup> (cm <sup>3</sup> /g)	Average pore size (nm)
Ni*	0.3	0.0019	66.6
Fe*	0.6	0.0029	89.6
Mn*	1.1	0.0036	42.8
Mn	0.6	-	-

a: The BET surface area of other samples was less than 0.3 m<sup>2</sup>/g.

b: The total pore volume was estimated from the adsorption branch at relative pressures ranging from 0.05 to 0.99.

**TableS10** Summary of peak distribution of C 1s and N 1s

Samples	C 1s (%)			N 1s (%)		
	C-C	C-N/C-O	O=C	Pyrrole N	Pyridine N	Graphite N
APA-2	46	40	14	67	28	5
Mn*	57	30	13	48	39	13
Mn	63	24	13	47	25	28
MnO	62	26	13	44	29	27

**TableS11** Summary of peak distribution of O 1s

Samples	O 1s (%)		
	C-O/C-OH	COOH	C=O
APA-2	74	24	2
Mn*	75	16	9
Mn	80	13	7
MnO	87	10	3

**TableS12** The results of impedances of all samples

Samples	$R_s$ ( $\Omega$ )	$R_1$ ( $\Omega$ )	$R_2$ ( $\Omega$ )
APA-2	2.57	0.28	0.48
Mn*	2.00	0.31	0.28
Mn	2.34	0.29	0.39
MnO	2.30	0.25	0.47

**Table S13.** Comparisons of OER catalytic activities of this work with that of the other similar catalysts.

Sample	$\eta_{10}$ (mV)	Loading (mg cm <sup>-2</sup> )	Electrolyte	Ref.
MnO	420	0.46	1.0 M KOH	This work
APA-2	453	0.46	1.0 M KOH	This work
BM30	474	0.46	1.0 M KOH	This work
AP	490	0.46	1.0 M KOH	This work
Co NP/NC-700	430	0.18	1.0 M KOH	[1]
Co/Zn@NC@MWCNTs	430	0.20	1.0 M KOH	[2]
CoFe-LDH/MWCNT/rGO	430	0.14	1.0 M KOH	[3]
Microwave treated carbon cloth	524	No	0.5 M H <sub>2</sub> SO <sub>4</sub>	[4]
CoW@ACSF	492	0.20	1.0 M KOH	[5]
CoSb/NC-0.05	430	0.22	1.0 M KOH	[6]
Co@NCS	430	No	0.1 M KOH	[7]
C@CeO <sub>2</sub> /Co <sub>3</sub> O <sub>4</sub>	425	No	0.5 M H <sub>2</sub> SO <sub>4</sub>	[8]
Co-N/RGO-700	430	0.21	0.1 M KOH	[9]
Co@N-Carbon	400	0.21	1.0 M KOH	[10]

**Figures :**

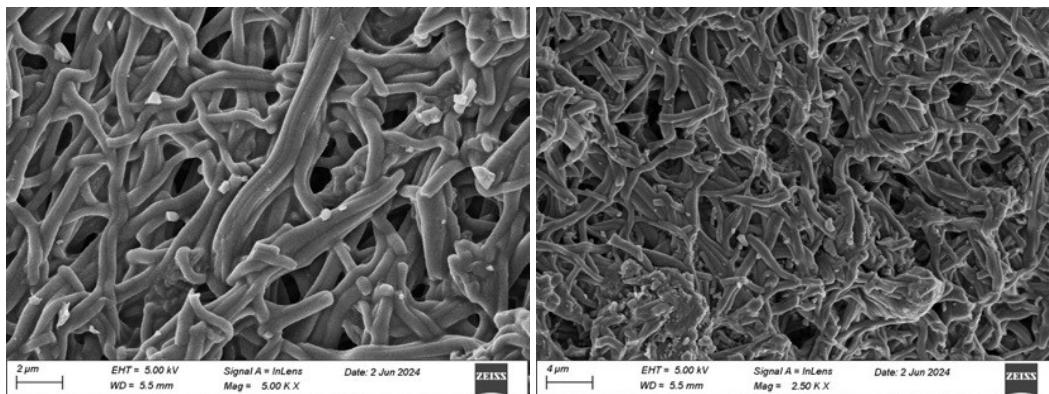


**Fig.S1** SEM images of APA-1.75 after pre-oxidation at 220 °C 1 hour and carbonization at 700 °C.

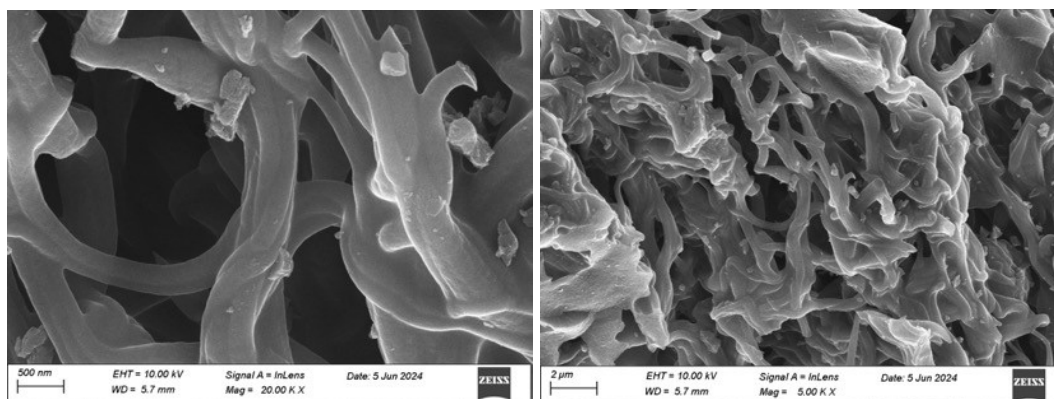


**Fig.S2** SEM images of APA-1.75 after pre-oxidation at 220 °C 1 hour and carbonization at 800 °C.

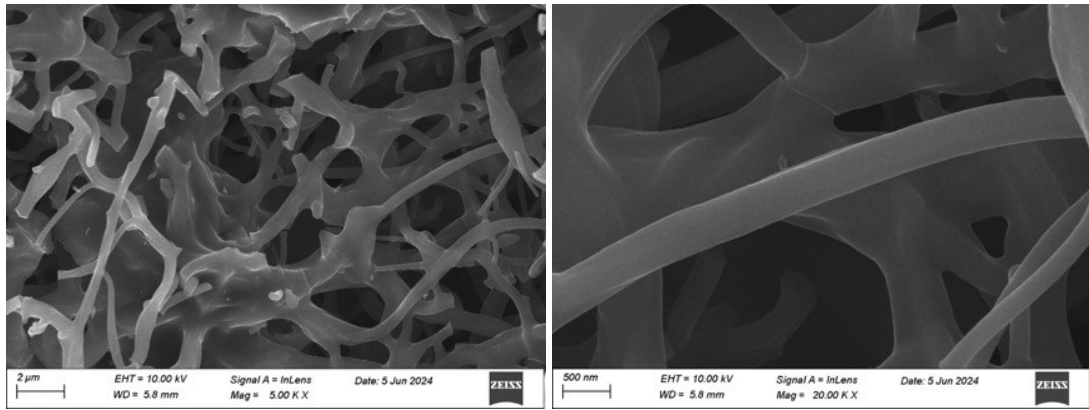


**Fig.S3** SEM images of APA-1.75 after pre-oxidation at 220 °C 1 hour and carbonization at 900 °C.

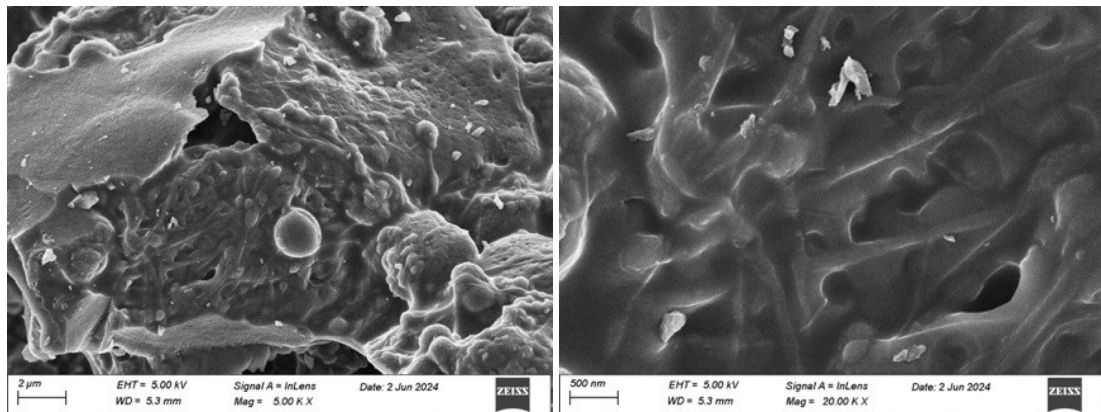


**Fig.S4** SEM images of APA-3 after pre-oxidation at 220 °C 1 hour and carbonization at 700 °C.

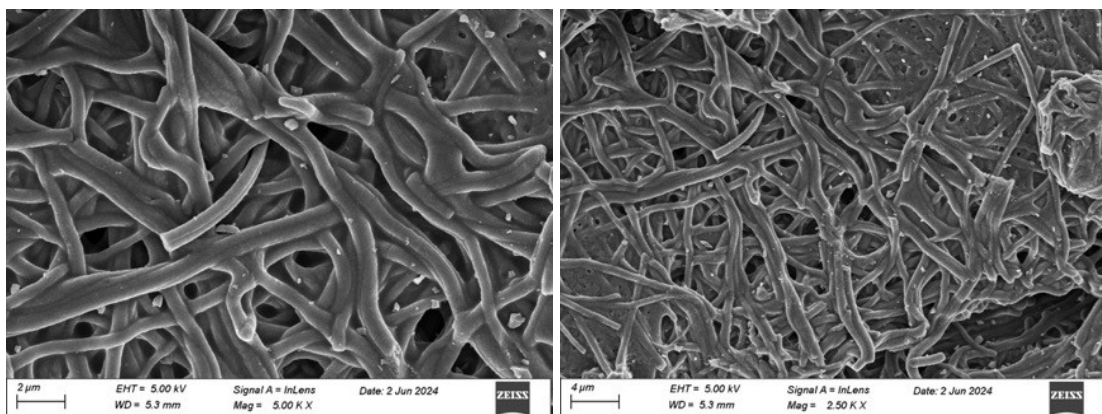


**Fig.S5** SEM images of APA-2 after pre-oxidation at 220 °C 1 hour and carbonization at 700 °C.

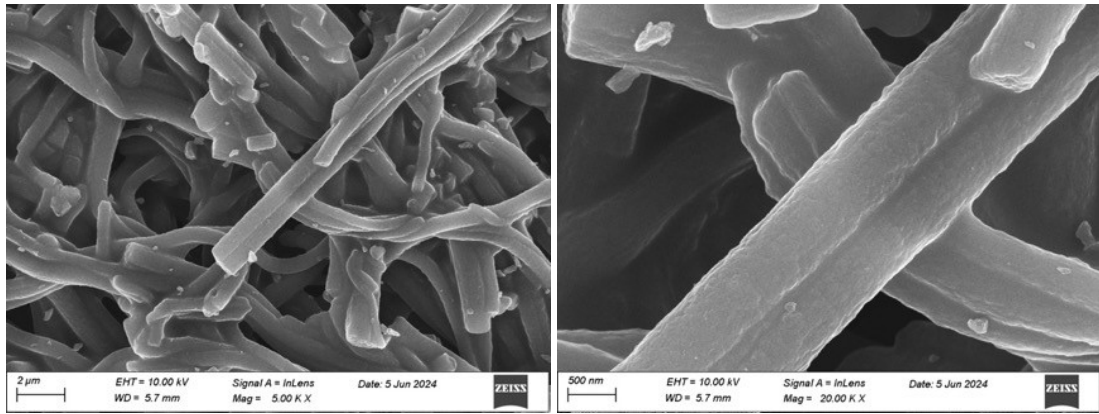


**Fig.S6** SEM images of APA-2 after pre-oxidation at 220 °C 1 hour and carbonization at 800 °C.

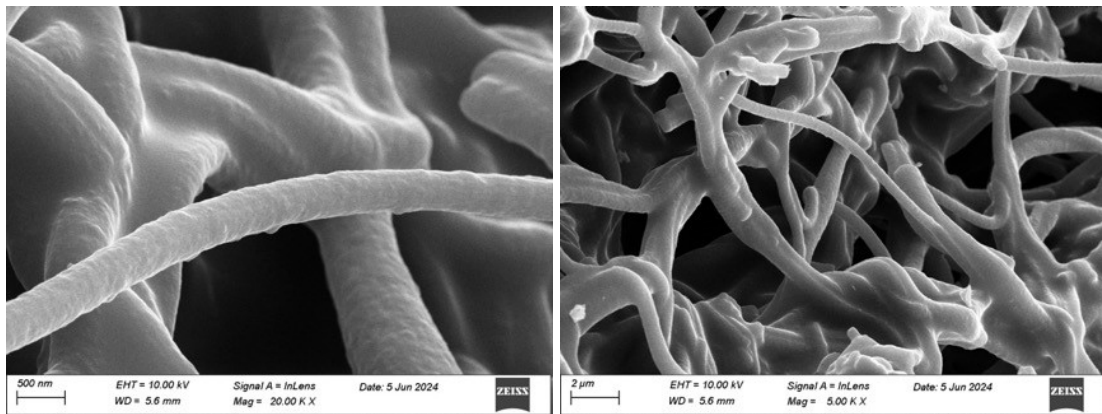


**Fig.S7** SEM images of APA-2 after pre-oxidation at 220 °C 1 hour and carbonization at 900 °C.

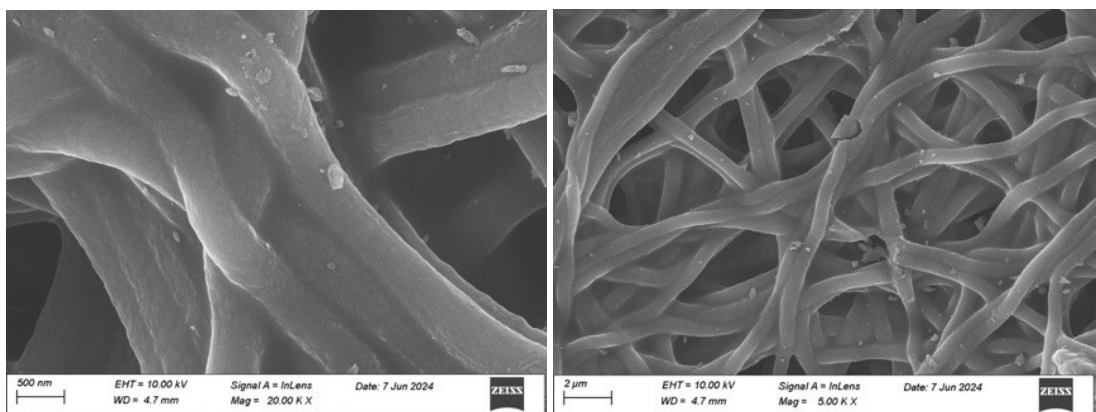


**Fig.S8** SEM images of APA-2 after pre-oxidation at 220 °C 3 hour and carbonization at 700 °C.

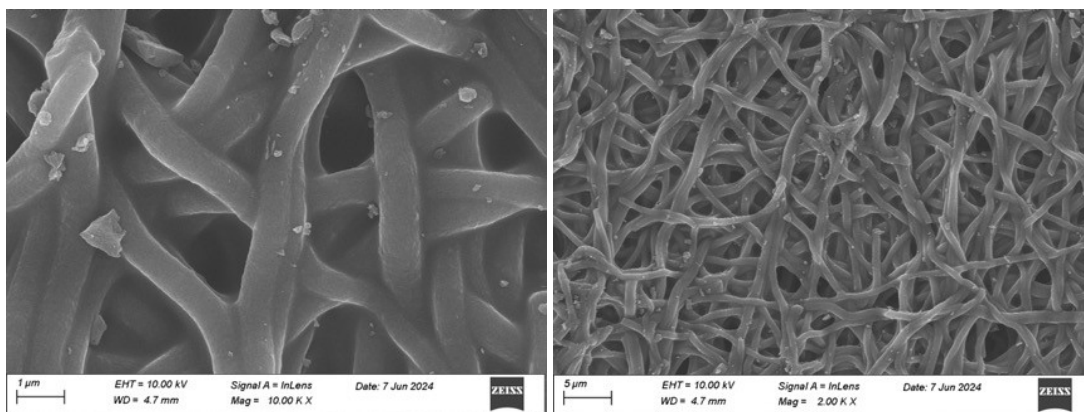


**Fig.S9** SEM images of APA-2 after pre-oxidation at 220 °C 3 hour and carbonization at 800 °C.

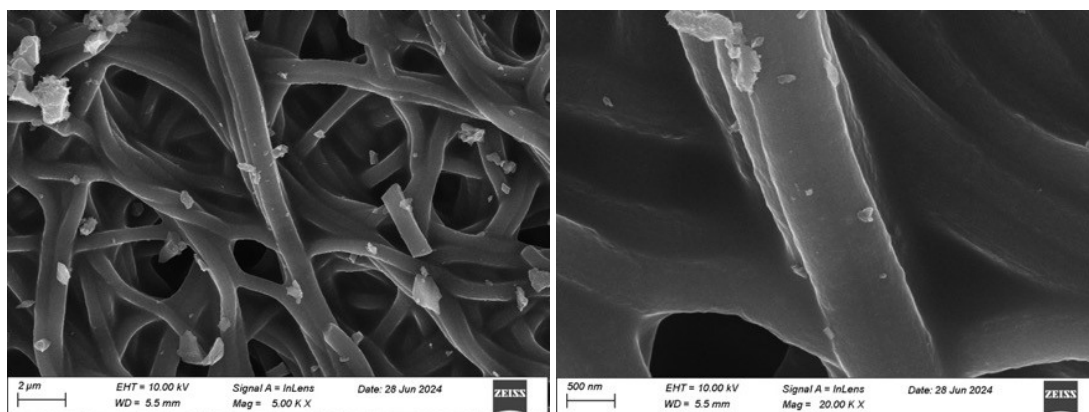


**Fig.S10** SEM images of APA-2 after pre-oxidation at 220 °C 3 hour and carbonization at 900 °C.

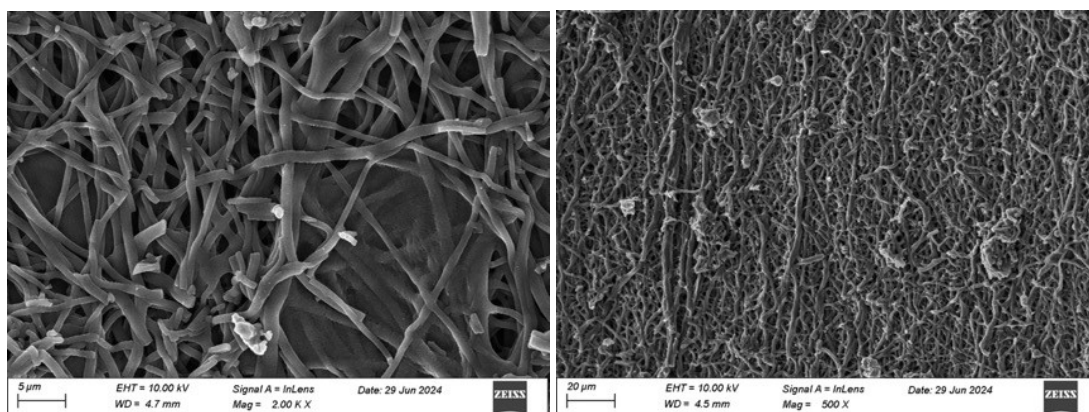


**Fig.S11** SEM images of APA-2 after pre-oxidation at 190 °C 1 hour and carbonization at 800 °C.

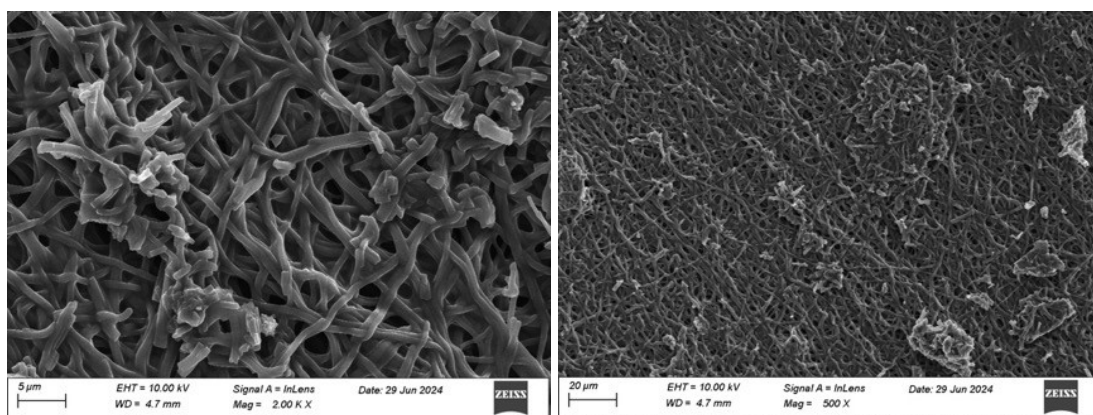


**Fig.S12** SEM images of APA-2 after pre-oxidation at 200 °C 1 hour and carbonization at 800 °C.

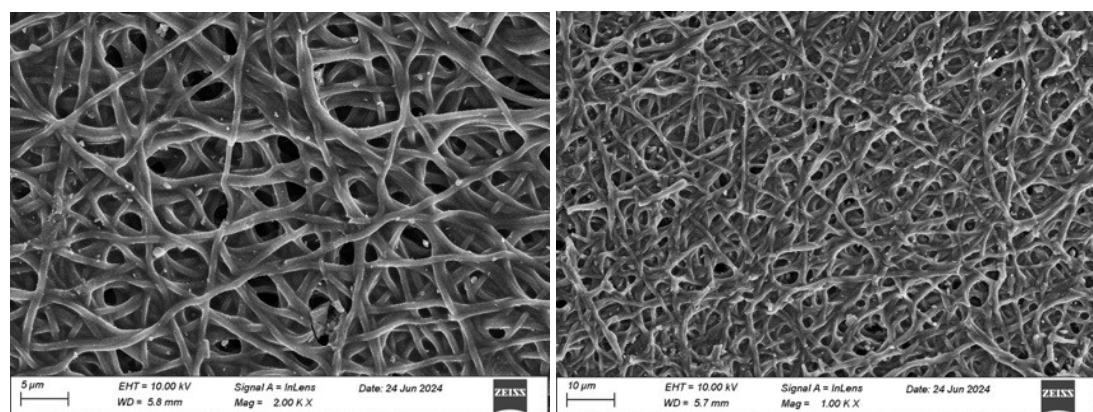


**Fig.S13** SEM images of APA-2 after pre-oxidation at 240 °C 3 hour and carbonization at 800 °C.

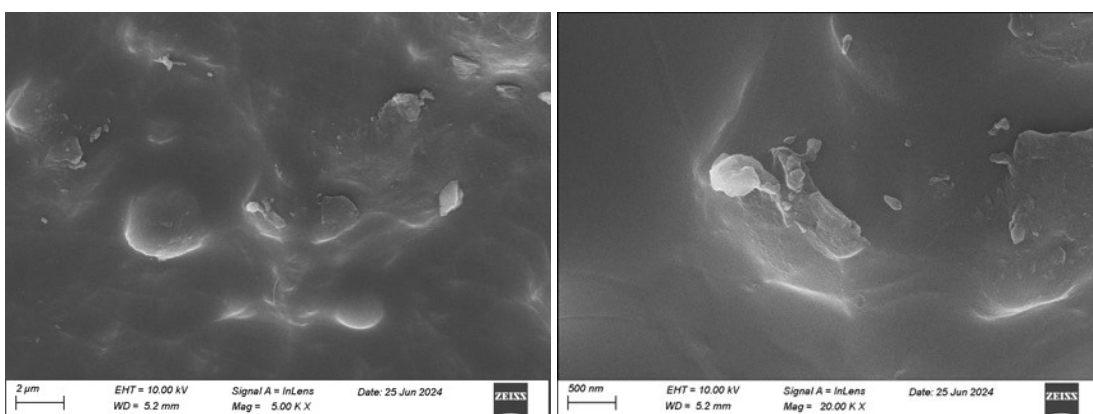


**Fig.S14** SEM images of APA-2 after pre-oxidation at 260 °C 3 hour and carbonization at 800 °C.

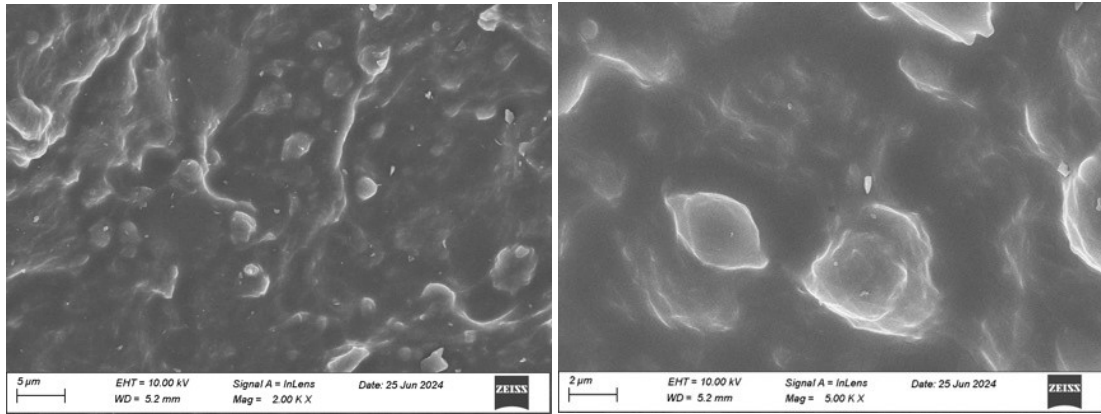


**Fig.S15** SEM images of APA-2 after pre-oxidation at 280 °C 3 hour and carbonization at 800 °C.

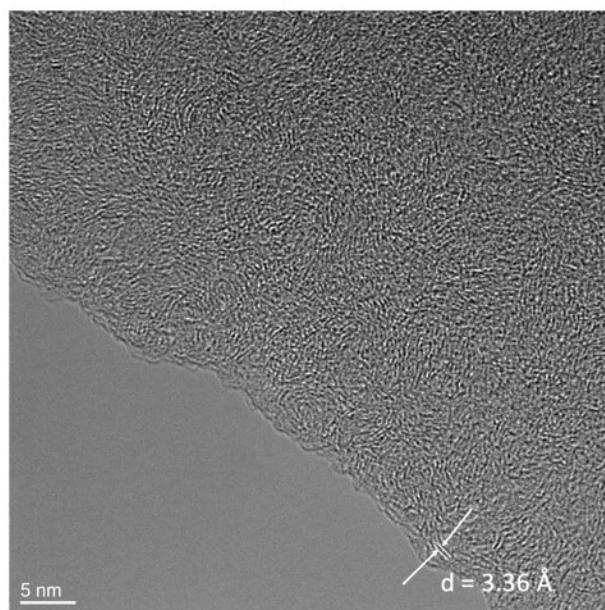


**Fig.S16** HRTEM image of APA-2 after pre-oxidation at 220 °C 3 hour and carbonization at 800 °C.

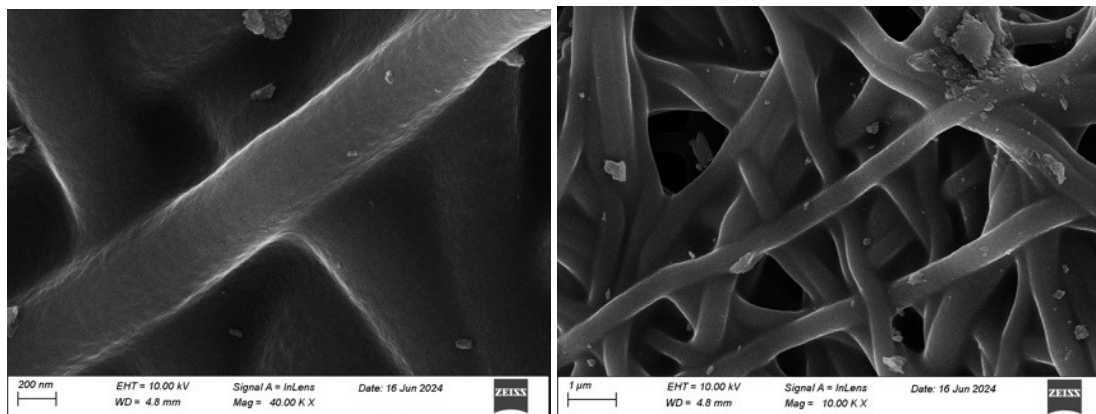


**Fig.S17** SEM images of Co\* after pre-oxidation at 220 °C 3 hour and carbonization at 800 °C.

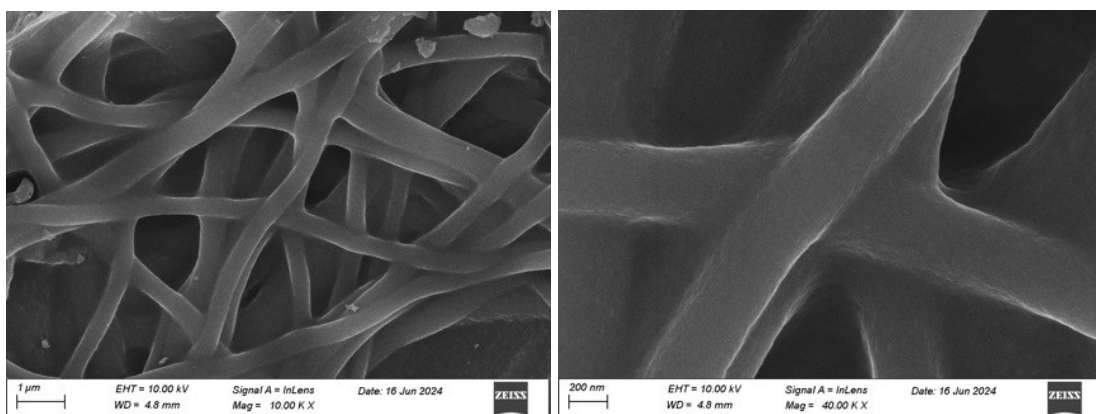


**Fig.S18** SEM images of Ni\* after pre-oxidation at 220 °C 3 hour and carbonization at 800 °C.

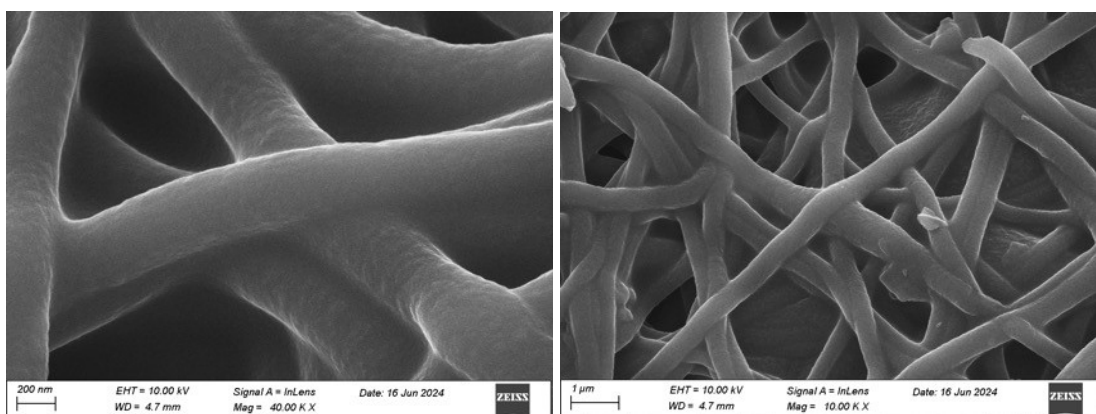


**Fig.S19** SEM images of Fe\* after pre-oxidation at 220 °C 3 hour and carbonization at 800 °C.

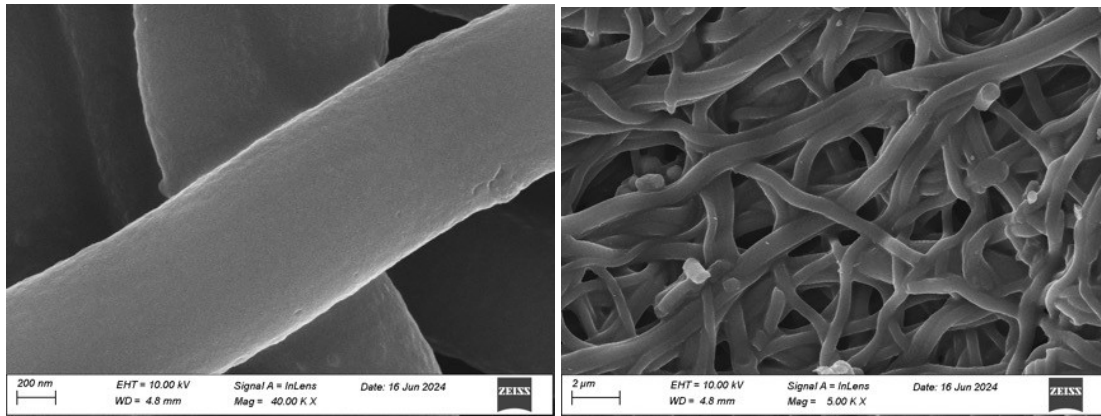


**Fig.S20** SEM images of Mn\* after pre-oxidation at 220 °C 3 hour and carbonization at 800 °C.

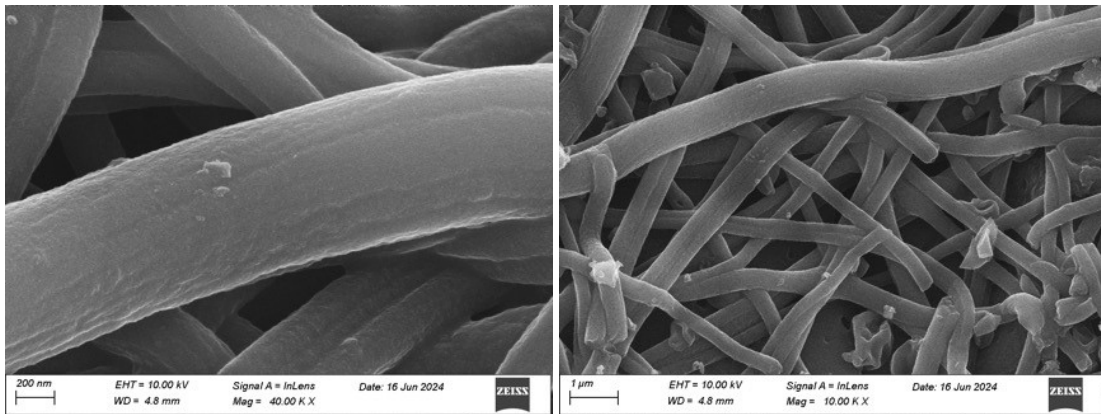


**Fig.S21** SEM images of Ni after pre-oxidation at 220 °C 3 hour and carbonization at 800 °C.

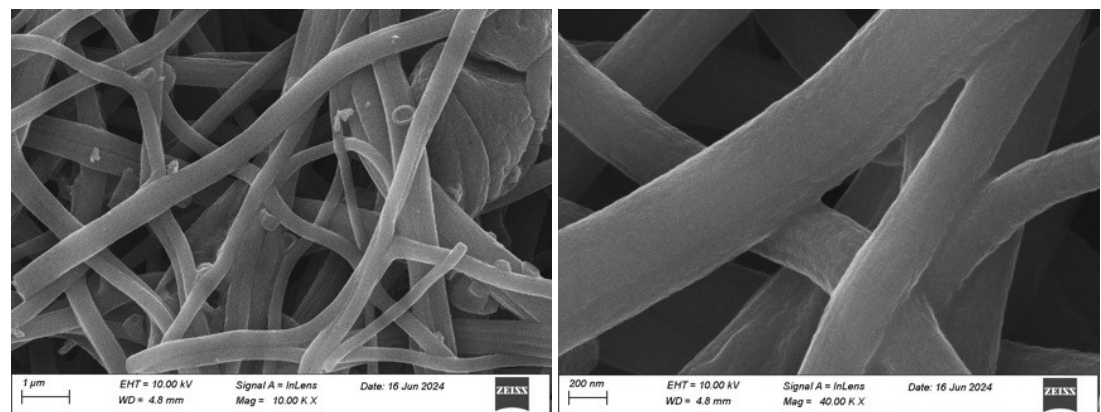


**Fig.S22** SEM images of Fe after pre-oxidation at 220 °C 3 hour and carbonization at 800 °C.

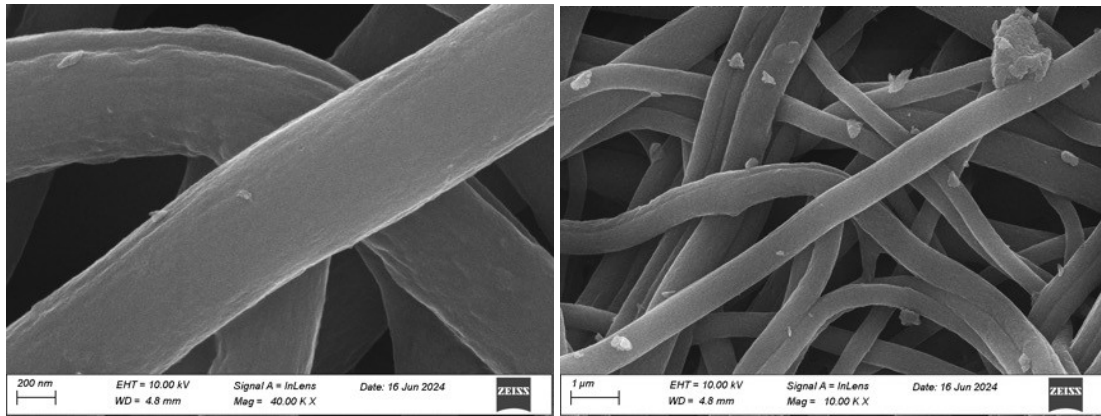


**Fig.S23** SEM images of Mn after pre-oxidation at 220 °C 3 hour and carbonization at 800 °C.

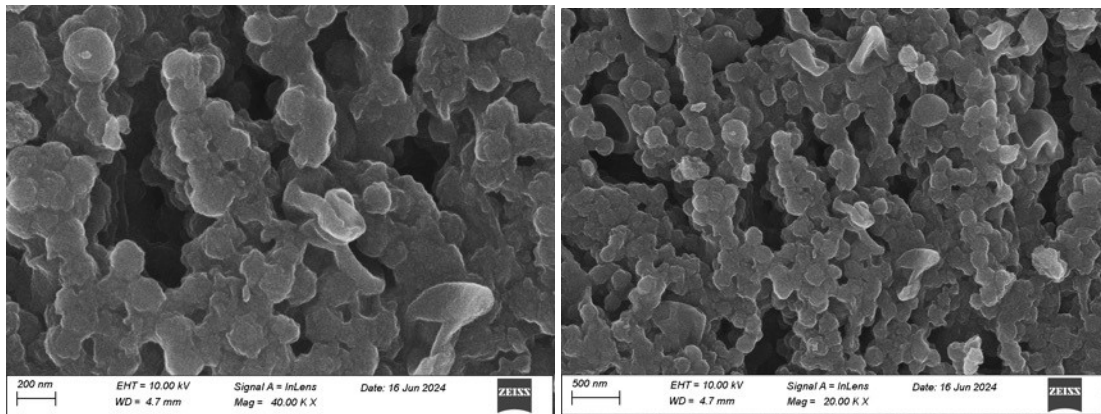


**Fig.S24** SEM images of Co after pre-oxidation at 220 °C 3 hour and carbonization at 800 °C

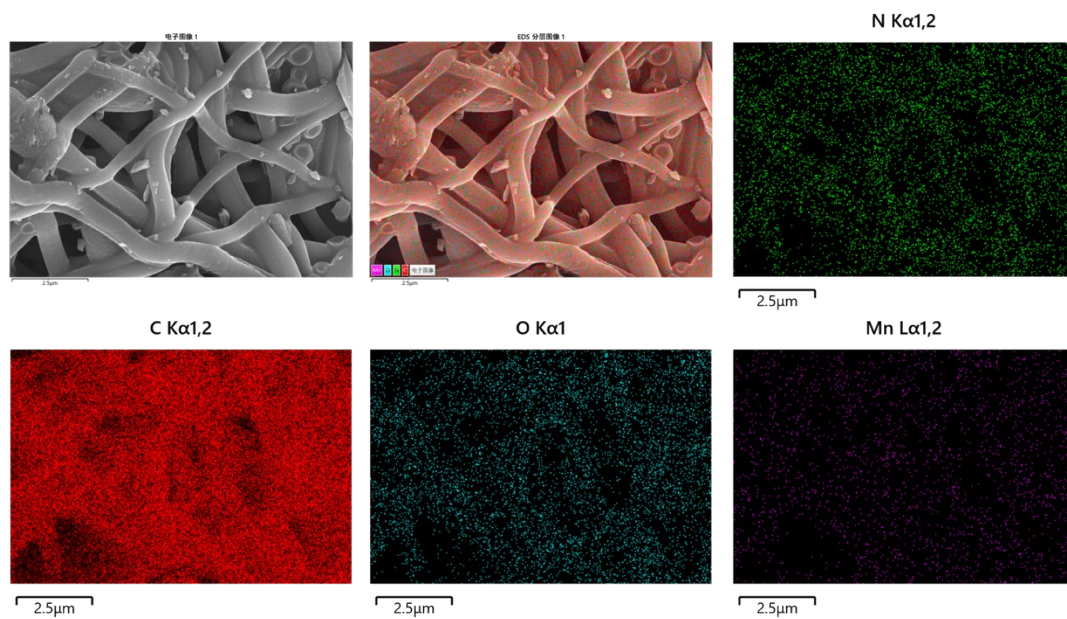


**Fig.S25** SEM and corresponding EDS elemental (C, N, O and Mn) mapping images of Mn\* after pre-oxidation at 220 °C 3 hour and carbonization at 800 °C.

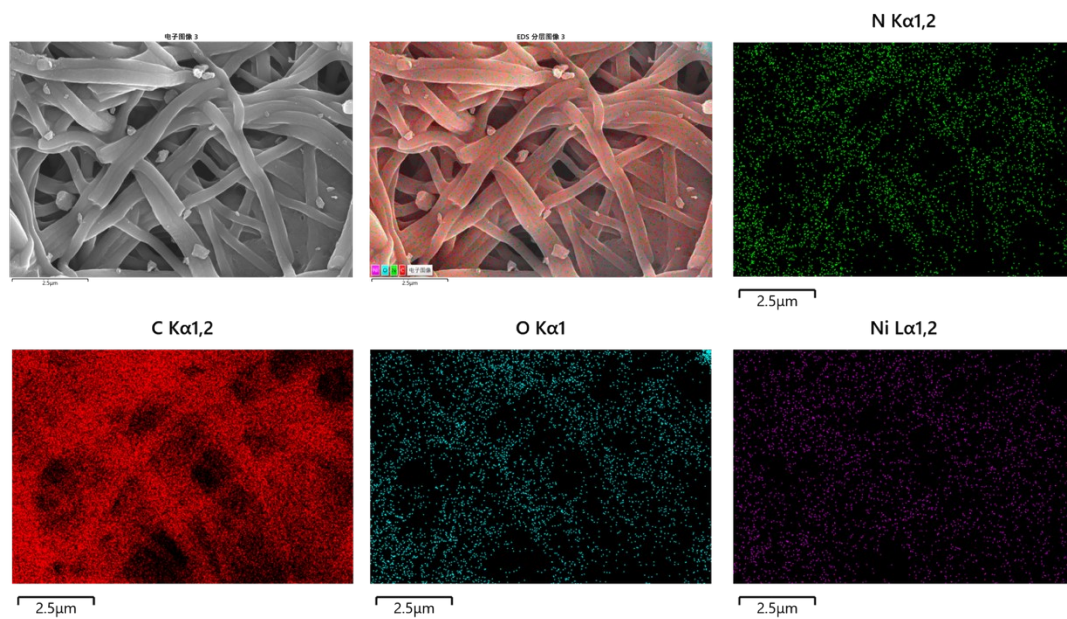


**Fig.S26** SEM and corresponding EDS elemental (C, N, O and Mn) mapping images of Ni after pre-oxidation at 220 °C 3 hour and carbonization at 800 °C.

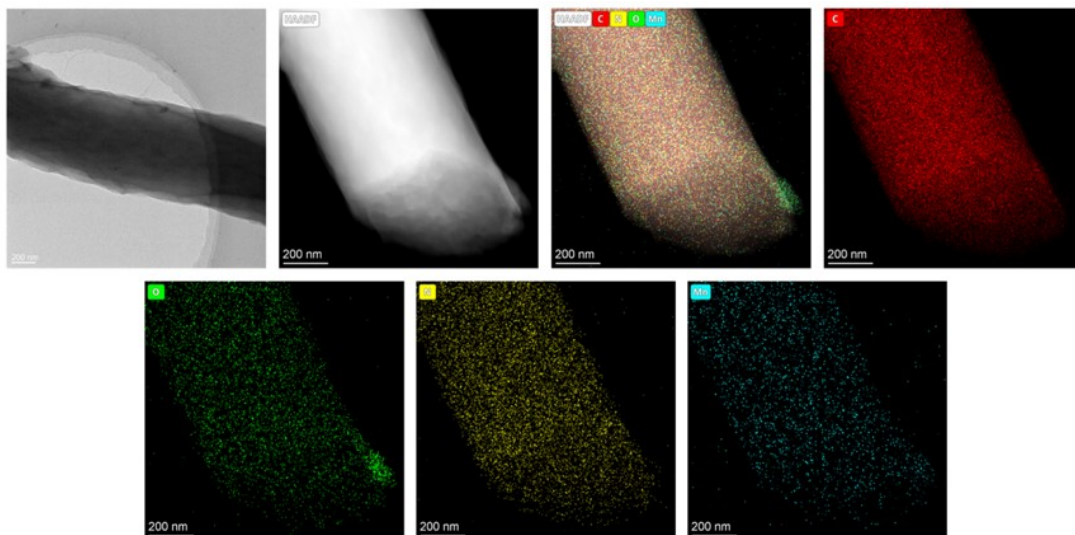


**Fig.S27** HRTEM and HADDF-mapping images (C, N, O and Mn) of Mn after pre-oxidation at 220 °C 3 hour and carbonization at 800 °C.

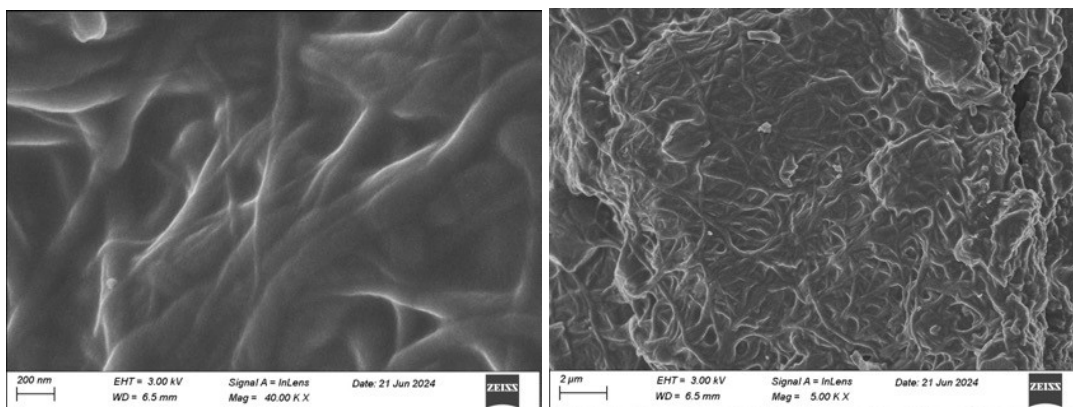


**Fig.S28** SEM images of MnO after pre-oxidation at 220 °C 3 hour and carbonization at 800 °C.

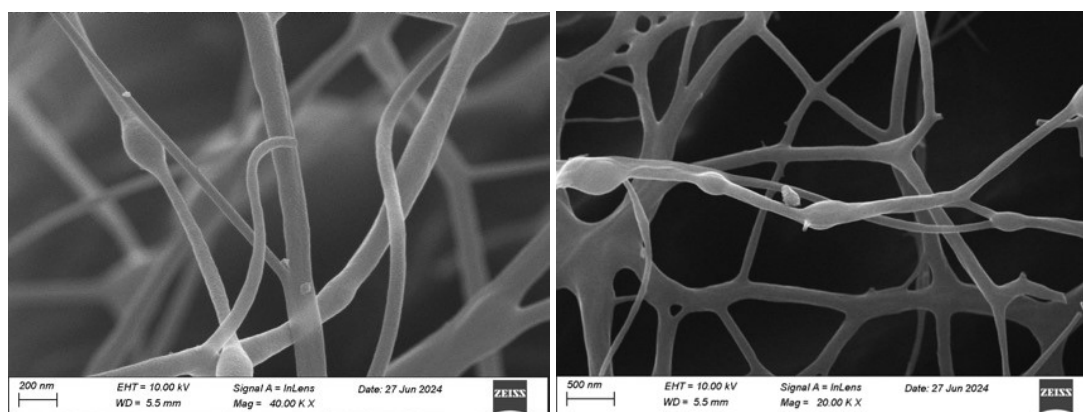


**Fig.S29** SEM images of MnO after pre-oxidation at 220 °C 3 hour and carbonization at 900 °C.

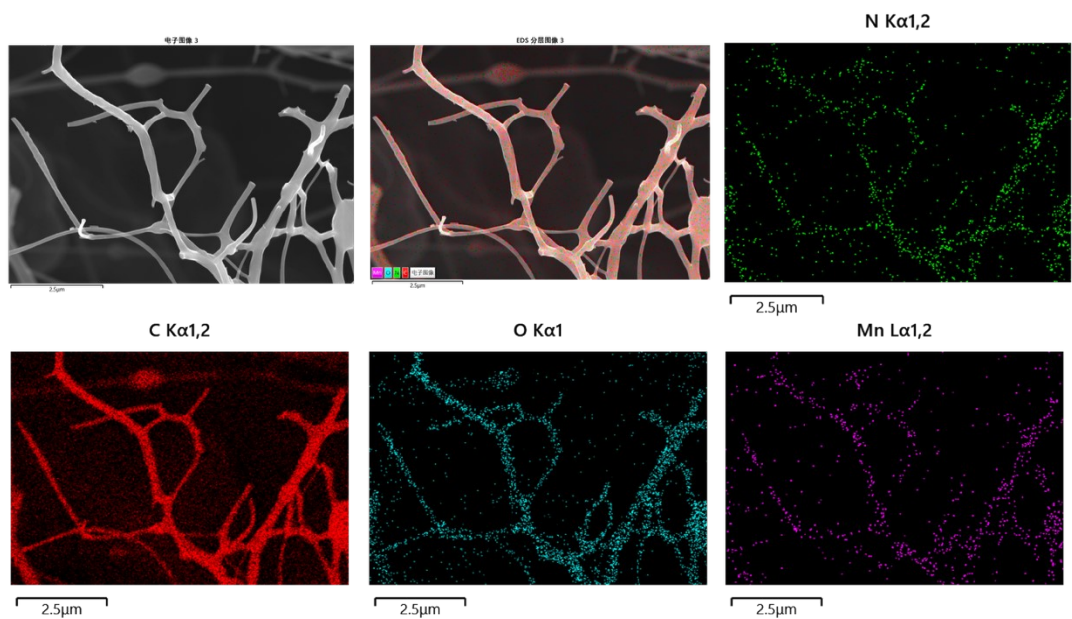


**Fig.S30** SEM and corresponding EDS elemental (C, N, O and Mn) mapping images of MnO after pre-oxidation at 220 °C 3 hour and carbonization at 900 °C.

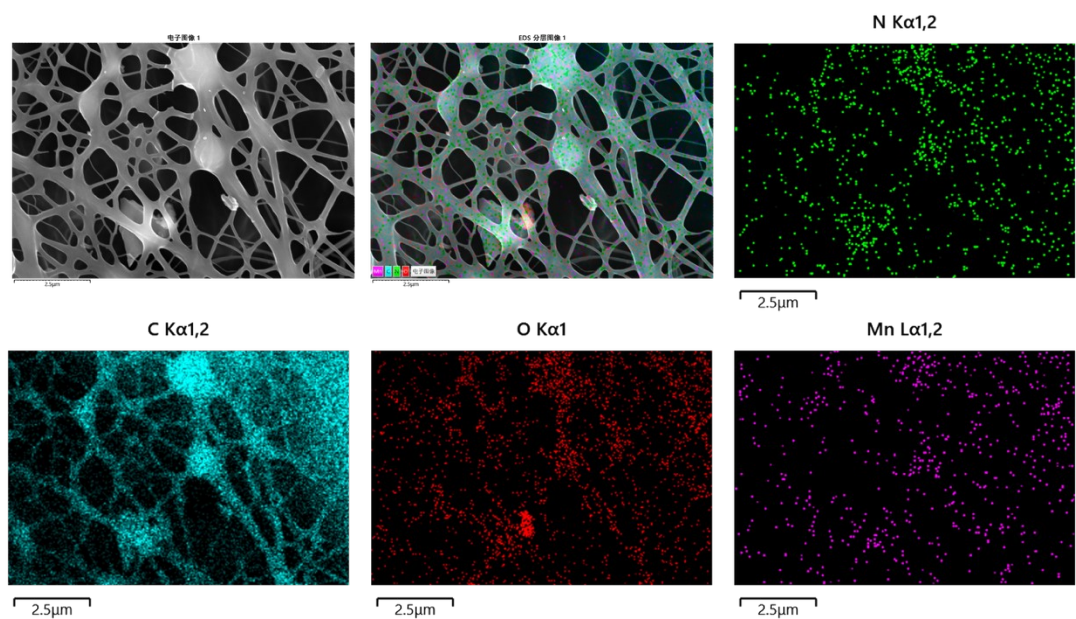


**Fig.S31** SEM and corresponding EDS elemental (C, N, O and Mn) mapping images of MnO after pre-oxidation at 220 °C 3 hour and carbonization at 900 °C.

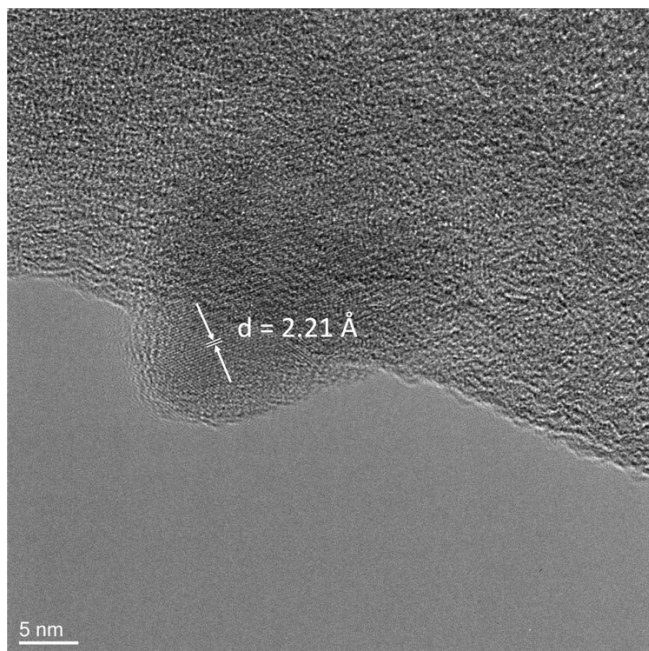


**Fig.S32** HRTEM image of MnO after pre-oxidation at 220 °C 3 hour and carbonization at 900 °C.

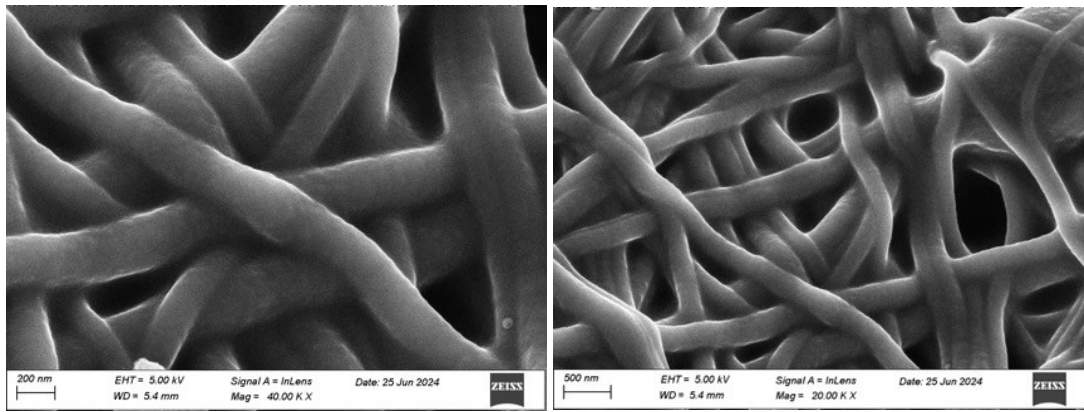


**Fig.S33** SEM images of CaO after pre-oxidation at 220 °C 3 hour and carbonization at 800 °C.

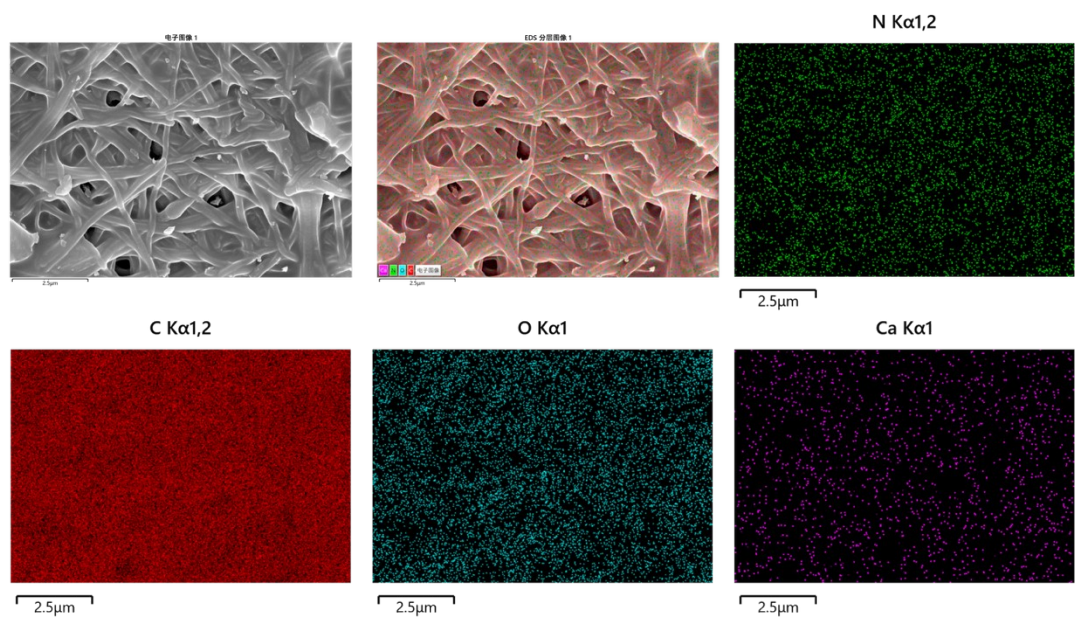


**Fig.S34** SEM and corresponding EDS elemental (C, N, O and Mn) mapping images of CaO after pre-oxidation at 220 °C 3 hour and carbonization at 800 °C.

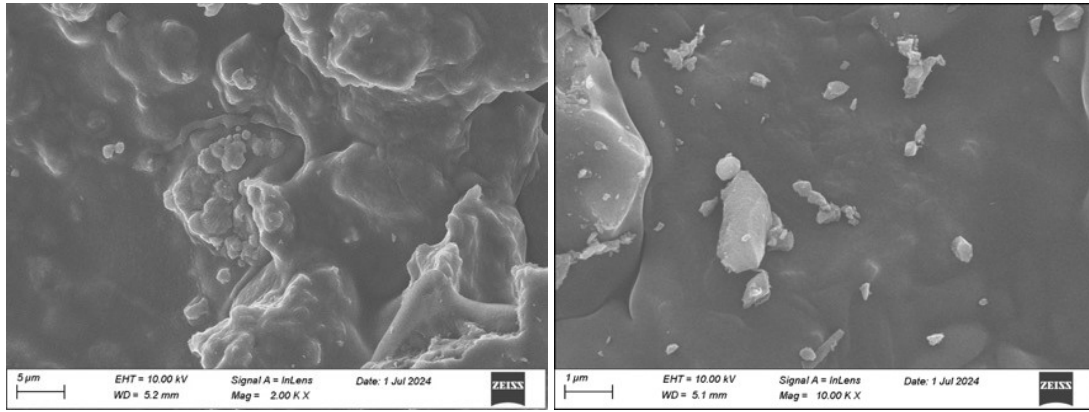


**Fig.S35** SEM images of CaO after pre-oxidation at 220 °C 3 hour and carbonization at 900 °C.

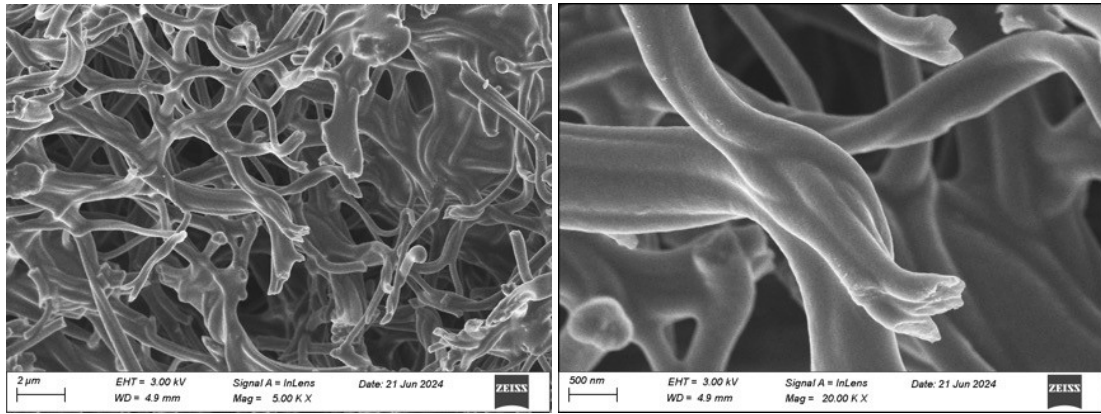


**Fig.S36** SEM images of  $\text{Al}_2\text{O}_3$  after pre-oxidation at 220 °C 3 hour and carbonization at 800 °C.

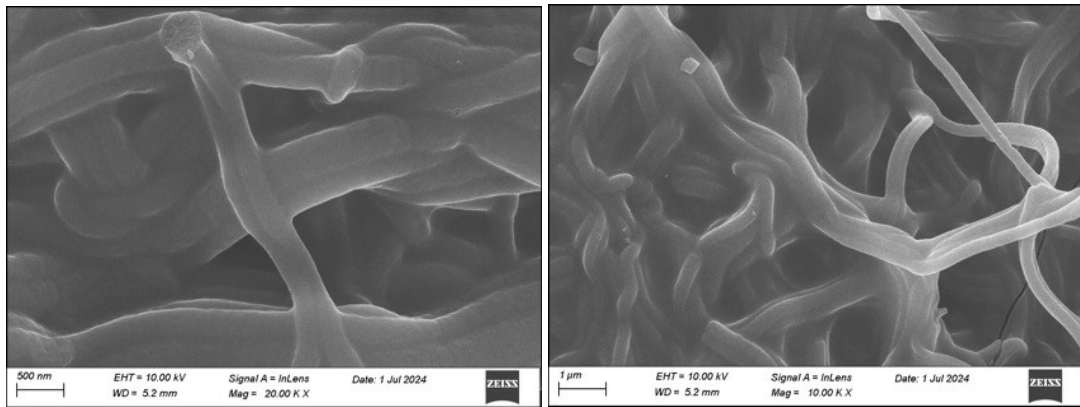


**Fig.S37** SEM images of  $\text{Al}_2\text{O}_3$  after pre-oxidation at 220 °C 3 hour and carbonization at 900 °C.

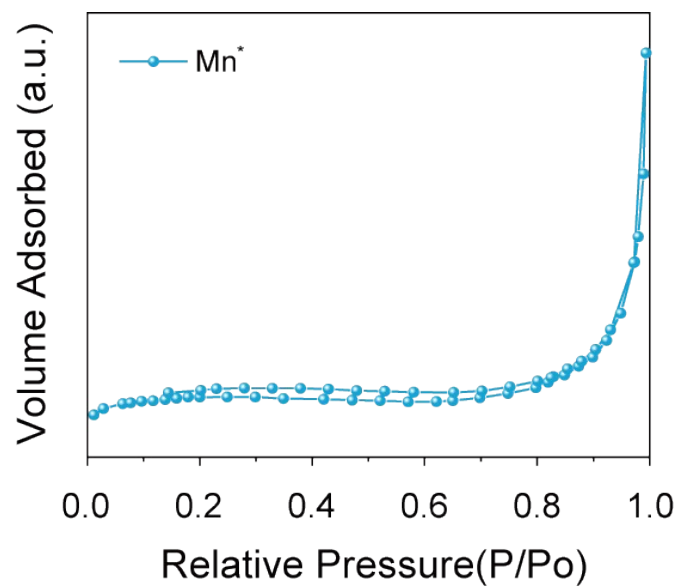


**Fig.S38** N<sub>2</sub> sorption isotherm (77 K) curves of Mn\*. The BET surface area of other samples was less than 1 m<sup>2</sup>/g.

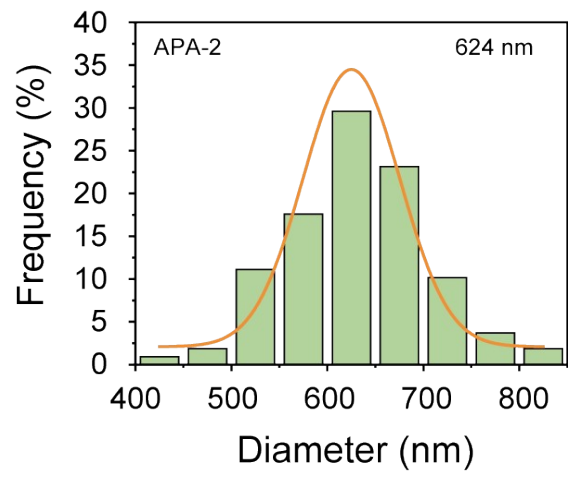


**Fig.S39** Nanofiber diameter distribution of APA-2.

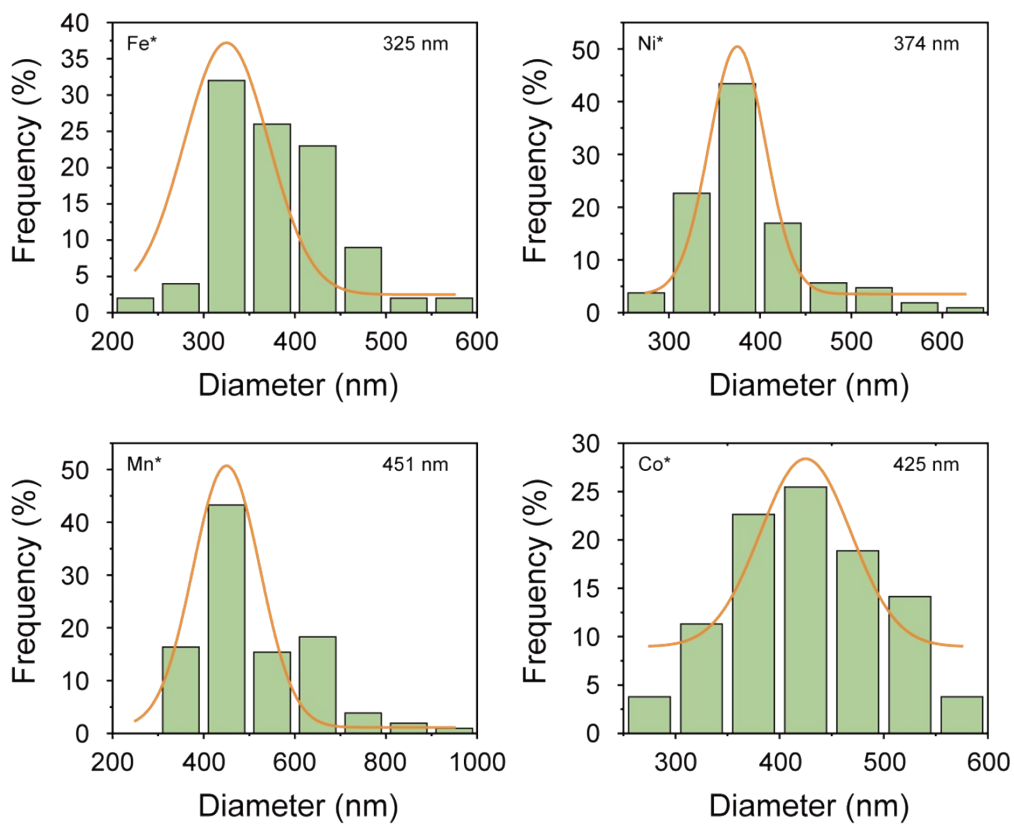


**Fig.S40** Nanofiber diameter distribution of Metalloporphyrin@APA-2.

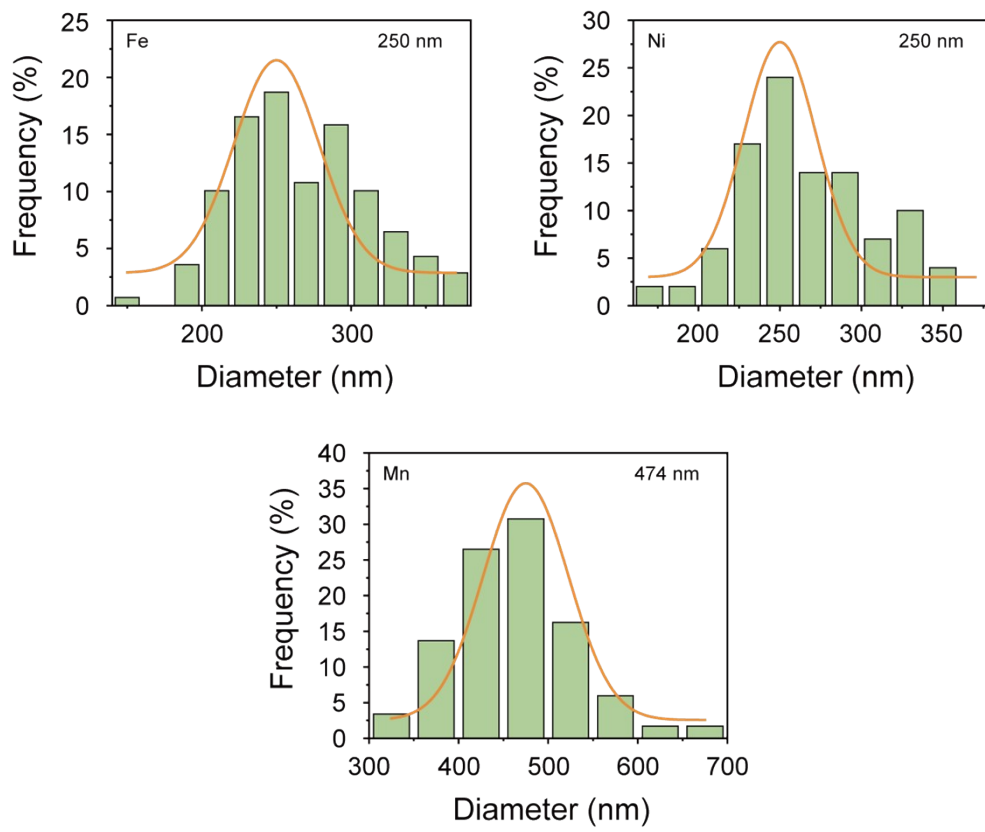


**Fig.S41** Nanofiber diameter distribution of Nitrate@APA-2.

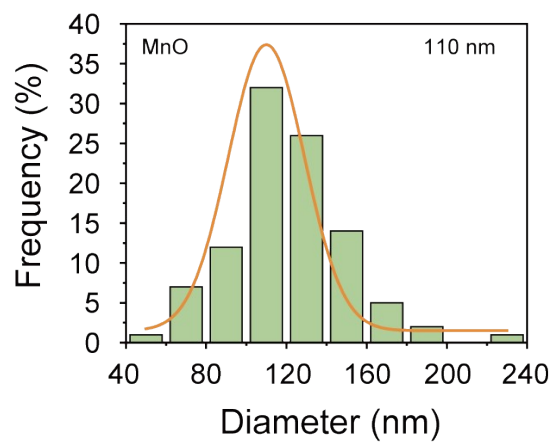


**Fig.S42** Nanofiber diameter distribution of Oxides@APA-2.

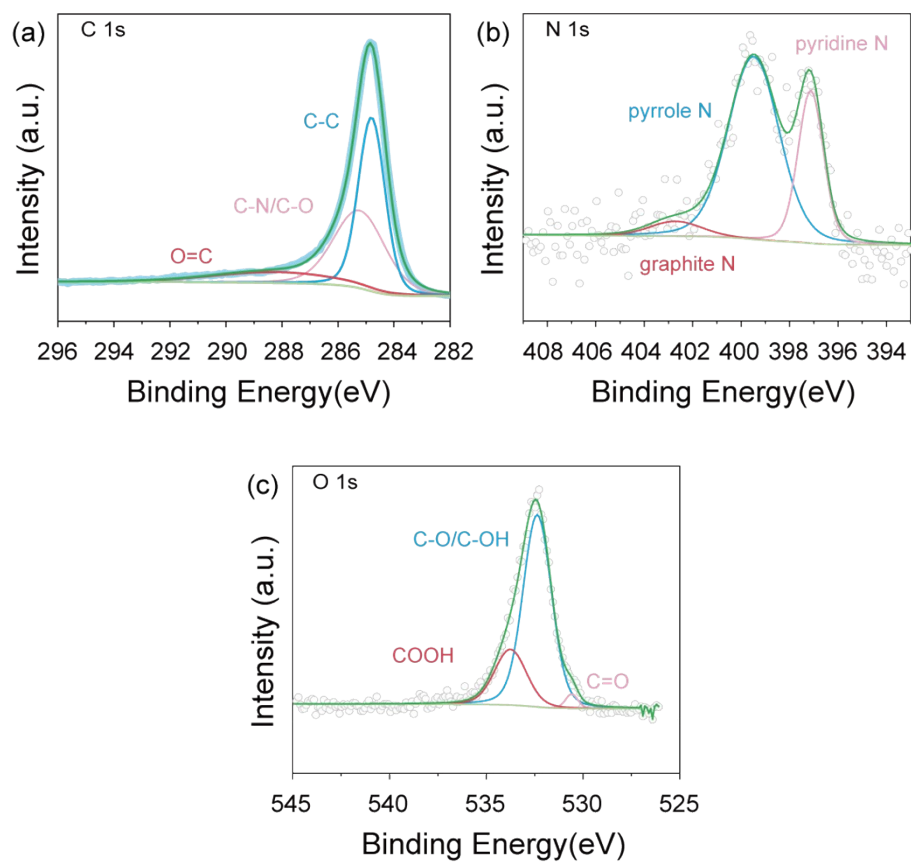


**Fig.S43** XPS spectra for (a) C 1s , (b) N 1s and (c) O 1s of APA-2.

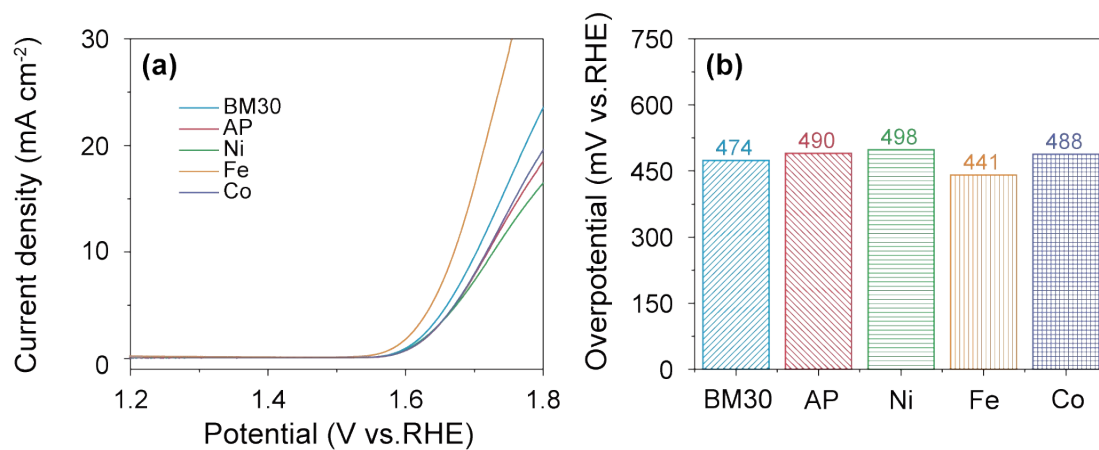


**Fig.S44** OER electrocatalytic performance of the catalysts in 1.0 M KOH solution. (a) Polarization curves and the corresponding (b) overpotential plots for BM30, AP, Ni, Fe and Co.

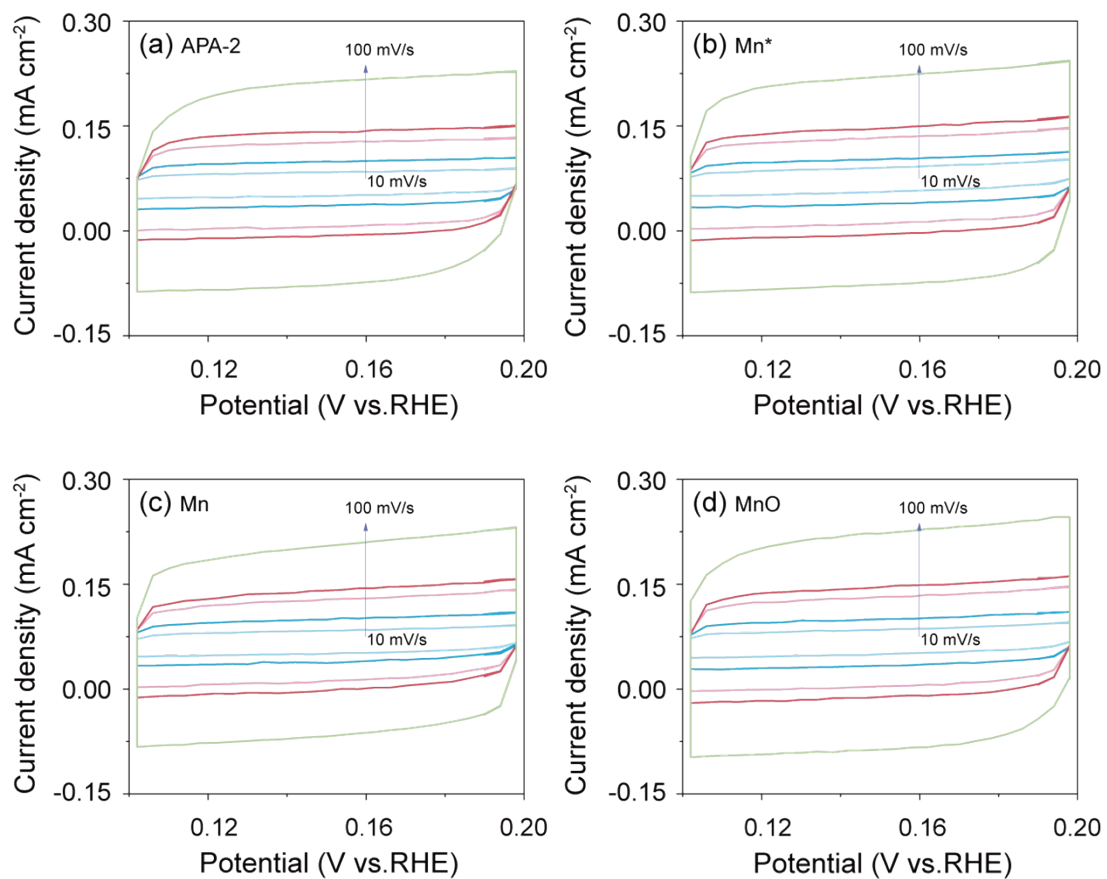


**Fig.S45** Cyclic voltammetry curves for (a) APA-2, (b) Mn\*, (c) Mn and (d) MnO performed at different scan rates.

## Reference :

1. J. Zhao, F. Rong, Y. Yao, et al., Co NP/NC hollow nanoparticles derived from yolk-shell structured ZIFs@polydopamine as bifunctional electrocatalysts for water oxidation and oxygen reduction reactions, *J. Energy Chem.*, 2018, **27**, 1261-1267.
2. T. H. Chen, C. S. Ni, C. Y. Lai, et al., Enhanced oxygen evolution and power density of Co/Zn@NC@MWCNTs for the application of zinc-air batteries, *J. Colloid Interface Sci.*, 2025, **679**, 119-131.
3. Y. J. Yang, M. Duan, C. Yan, et al., Facile synthesis of CoFe-LDH/MWCNT/rGO nanocomposite as efficient bifunctional electrocatalysts for oxygen evolution and reduction, *J. Electroanal. Chem.*, 2020, **856**, 113697.
4. W. Zhang, Y. Li, Y. Xu, et al., Microwave Reaction: A Facile Economic and Green Method to Synthesize Oxygen-Decorated Graphene from Carbon Cloth for Oxygen Electrocatalysis, *ChemCatChem*, 2018, **10**, 2305-2310.
5. H. He, Y. Zhang, W. Zhang, et al., Dual Metal-Loaded Porous Carbon Materials Derived from Silk Fibroin as Bifunctional Electrocatalysts for Hydrogen Evolution Reaction and Oxygen Evolution Reaction, *ACS Appl. Mater. Interfaces*, 2021, **13**, 30678-30692.
6. T. Gong, P. Sun, X. Xie, et al., Sb-modulated synthesis of novel CoSb alloy nanoparticles anchored on N-doped carbon as oxygen electrocatalysts, *Appl. Surf. Sci.*, 2021, **562**, 150112.
7. Y. Zhang, Y. Shen, S. Qiang, et al., Template-directed synthesis of Co, N-doped carbon spheres for efficient oxygen reduction reaction, *Inorg. Chem. Commun.*, 2025, **172**, 113678.
8. H. Li, Y. Yang, J. Zhang, et al., Boosting CeO<sub>2</sub>/Co<sub>3</sub>O<sub>4</sub> Heterojunctions Acidic Oxygen Evolution via Promoting OH Coverage, *ACS Appl. Energy Mater.*, 2023, **6**, 8949-8956.
9. N. Bhuvanendran, S. Ravichandran, S. Kumar R, et al., Boosting the oxygen bifunctional activity on cobalt nanocrystals/RGO with extended durability, *Mater. Today Sustain.*, 2023, **24**, 100596.

10. J. Cong, H. Xu, M. Lu, et al., Two-Dimensional Co@N-Carbon Nanocomposites Facilely Derived from Metal-Organic Framework Nanosheets for Efficient Bifunctional Electrocatalysis, *Chem. Asian J.*, 2018, **13**, 1485-1491.